Research Article

pISSN 2799-8525 · eISSN 2799-8681
J Powder Mater 2025;32(1):23-29

Journal of
Powder Materials

Comparative Study of Reduced Graphene Oxide Aerogels and Films for Supercapacitor Electrodes

Sunghee Choi[1], Seulgi Kim[1], Seojin Woo[1], Dongju Lee[1,2,*]

[1]Department of Urban, Energy, and Environmental Engineering, Chungbuk National University, Chungdae-ro 1, Seowon-Gu, Cheongju, Chungbuk 28644, Republic of Korea
[2]Department of Advanced Materials Engineering, Chungbuk National University, Chungdae-ro 1, Seowon-Gu, Cheongju, Chungbuk 28644, Republic of Korea

Supercapacitors, renowned for their high power density and rapid charge-discharge rates, are limited by their low energy density. This limitation has prompted the need for advanced electrode materials. The present study investigated reduced graphene oxide (rGO) in two distinct structures, as a film and as an aerogel, for use as supercapacitor electrodes. The rGO film, prepared by vacuum filtration and thermal reduction, exhibited a compact, lamellar structure, while the aerogel, synthesized through hydrothermal treatment, was a highly porous three-dimensional network. Electrochemical analyses demonstrated the aerogel's superior performance, as shown by a specific capacitance of 121.2 F/g at 5 mV/s, with 94% capacitance retention after 10,000 cycles. These findings emphasize the importance of structural design in optimizing ion accessibility and charge transfer. They also demonstrate the potential of rGO aerogels for increasing the energy storage efficiency of advanced supercapacitor systems.

Keywords: Reduced graphene oxide; Aerogel; Film; Supercapacitor

Received: December 5, 2024
Revised: January 23, 2025
Accepted: February 1, 2025

***Corresponding author:**
Dongju Lee
E-mail: dongjulee@chungbuk.ac.kr

1. Introduction

With the increasing global demand for sustainable and efficient energy storage systems, improving the technologies that address diverse energy requirements has become an area of extensive research [1]. Among these technologies, lithium-ion batteries and supercapacitors are leading candidates, each one offering distinct advantages. Lithium-ion batteries are renowned for their high energy density, making them suitable for long-term energy storage, whereas supercapacitors excel in applications requiring high power density, rapid charge-discharge rates, and an exceptional cycle life [2]. Expanding the applicability of supercapacitors across a wider range of fields requires complementing their inherent advantages of high power density and long cycle life with an improvement of their energy density.

The performance of supercapacitors is largely governed by the choice of electrode materials, which directly influence energy and power capabilities. Carbon-based materials, including activated carbon, carbon nanotubes, and graphene, are extensively used due to their high specific surface area and excellent conductivity [3]. In particular, graphene has gained significant attention given its mechanical strength [4], high electrical conductivity [5], and extensive surface area [6]. These properties make graphene a highly promising candidate for electric double-layer capacitors (EDLCs) [7]. However, the strong van der Waals forces between graphene sheets often lead to aggregation, reducing the effective surface area and limiting the electrochemical performance [8]. Strategies that have been explored to prevent aggregation include the introduction of structural modifications and the incorporation of spacers [9]. Such methods are aimed at enhancing the specific surface area and improving the overall electrochemical properties of graphene.

In this study, a freestanding rGO film and a freestanding rGO aerogel were synthesized and their properties as supercapacitor electrodes were then compared. The structural differ-

https://doi.org/10.4150/jpm.2024.00472
© 2025 The Korean Powder Metallurgy & Materials Institute

ence was found to play a critical role in EDLC behavior, with the rGO aerogel demonstrating a higher specific capacitance of 121.2 F/g at 5 mV/s, outperforming the rGO film. The enhanced performance of the aerogel can be attributed to its superior surface area and efficient ion transport pathways. These findings highlight the importance of structural design in optimizing rGO electrodes for energy storage systems requiring both high energy and high power densities.

2. Experimental Section

Synthesis of graphene oxide (GO): GO was synthesized using Hummers' method. Briefly, 1 g of graphite flakes (Bay Carbon Inc) were placed into a flask, followed by the addition of 40 mL of concentrated H_2SO_4 (SAMCHUN) under an ice bath. After the mixture had been stirred for several minutes, 3.5 g of $KMnO_4$ (DAEJUNG) was slowly added to the flask, followed by stirring at 35°C for 2 h. Next, 200 mL of deionized (DI) water was added gradually under continuous stirring, followed by the addition of 10 mL of H_2O_2 (Junsei). The resulting solution was washed with diluted HCl (Junsei) (DI water:HCl = 9:1) to remove residual metal ions and then rinsed repeatedly with DI water until the pH of the solution reached approximately 6. The product was dried in a vacuum oven at room temperature to obtain GO powders.

Synthesis of the reduced graphene oxide (rGO) film: The rGO film was prepared via vacuum filtration followed by thermal reduction. GO was dispersed in DI water at a concentration of 2 mg/mL and sonicated to ensure uniform dispersion. The resulting dispersion was subjected to vacuum filtration to form a compact film on a membrane. The obtained GO film was dried at room temperature before it was thermally reduced at 200°C for 2 h under atmospheric conditions.

Synthesis of the rGO aerogel: The rGO aerogel was fabricated according to the hydrothermal method. A GO dispersion (2 mg/mL) was prepared in DI water and transferred into a Teflon-lined autoclave. The autoclave was heated at 180°C for 2 h to induce the self-assembly and reduction of the gel. The resultant hydrogel was freeze-dried to obtain the rGO aerogel.

Materials characterization: The crystallographic structures of GO and rGO were investigated by X-ray diffractometry (XRD; JP/SmartLab, Rigaku). Morphology and size were characterized by transmission electron microscopy (JEM-ARM200F, JEOL), and the surface chemical composition, elemental states, and bonding environment of the materials by X-ray photoelectron spectroscopy (K-Alpha+, Thermo Fisher Scientific). The microstructures of the rGO aerogel and film were examined using field-emission scanning electron microscopy (Crossbeam 540, ZEISS). The Raman spectra were analyzed using a micro-Raman spectrometer (RAMANtouch, Nanophoton, Republic of Korea) with a 514 nm laser source. The specific surface area was calculated in Brunauer-Emmett-Teller analysis, using the nitrogen adsorption isotherm branch with nano-porosity (Miraesi, Republic of Korea).

Electrochemical measurement: The rGO aerogel was used as an electrode by compressing it at 10 MPa. Both the rGO aerogel and film electrodes were prepared with a diameter of 12.7 mm. The electrodes were tested in a two-electrode symmetric cell configuration using 1 M H_2SO_4 as the electrolyte. Electrochemical performance was evaluated using cyclic voltammetry (CV), galvanostatic charge/discharge (GCD), and electrochemical impedance spectroscopy (EIS) measurements, performed on a potentiostat (SP-50e, Bio-Logic). The specific capacitance (C_g) was calculated using the following equation:

$$C_g = \frac{2}{mv\Delta V}\int IdV$$

where m is the mass of the electrode, v is the scan rate, ΔV is the voltage window, and I is the discharge current. The EIS analysis was conducted at an amplitude of 20 mV and a frequency range of 100 mHz to 100 kHz.

3. Results and Discussion

Figure 1 shows the fabrication process of the rGO film and rGO aerogel. The rGO film was prepared by vacuum filtering a GO dispersion to form a compact film, followed by thermal reduction at high temperature to restore conductivity and reduce oxygen-containing functional groups. The rGO aerogel was prepared using a GO dispersion in a hydrothermal synthesis method. During the hydrothermal process, the rGO aerogel was reduced and self-assembled without the need for additional reductants.

The morphology of the GO and the resulting rGO was examined using TEM. Figure 2a shows the monolayer sheet morphology, typical of well-exfoliated GO. After thermal reduction, the morphology of the rGO was similar (Fig. 2b). The lateral size of both GO and rGO was approximately 1 μm, indicating that the reduction process did not significantly alter the sheet dimensions. The structural changes resulting from the reduction of GO to rGO were analyzed using XRD and Raman spectroscopy. Fig. 2c presents the XRD patterns of GO and rGO. In the GO spectrum, the prominent peak at 10.7° corresponded to

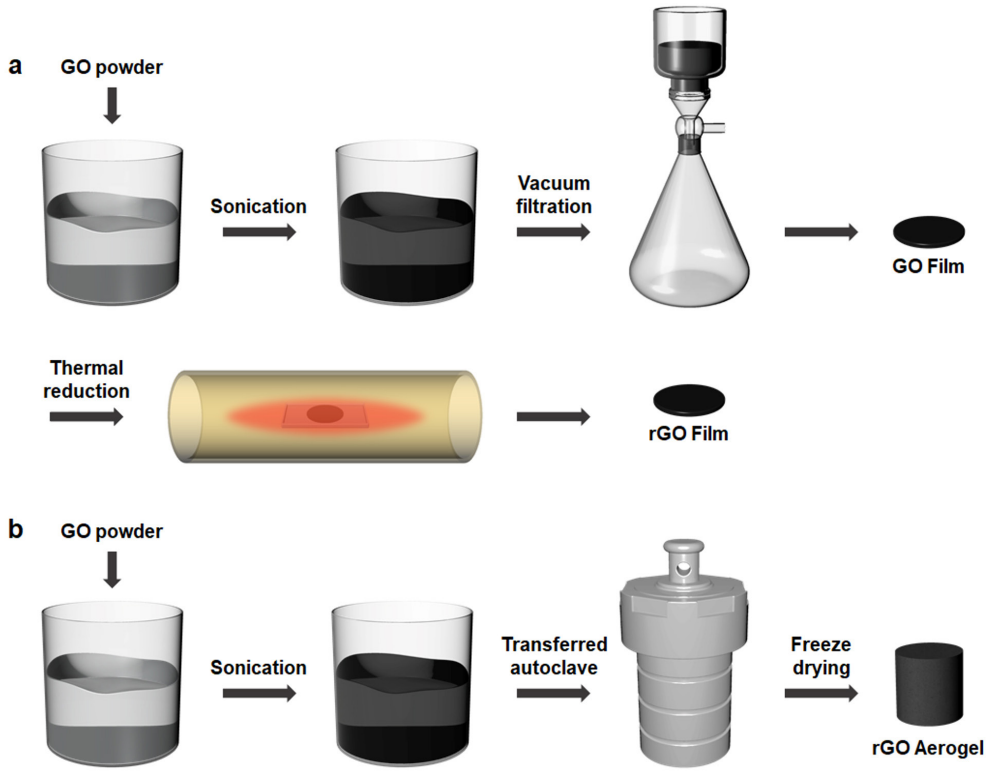

Fig. 1. A schematic illustration of the preparation process for (a) the reduced graphene oxide (rGO) film and (b) the rGO aerogel.

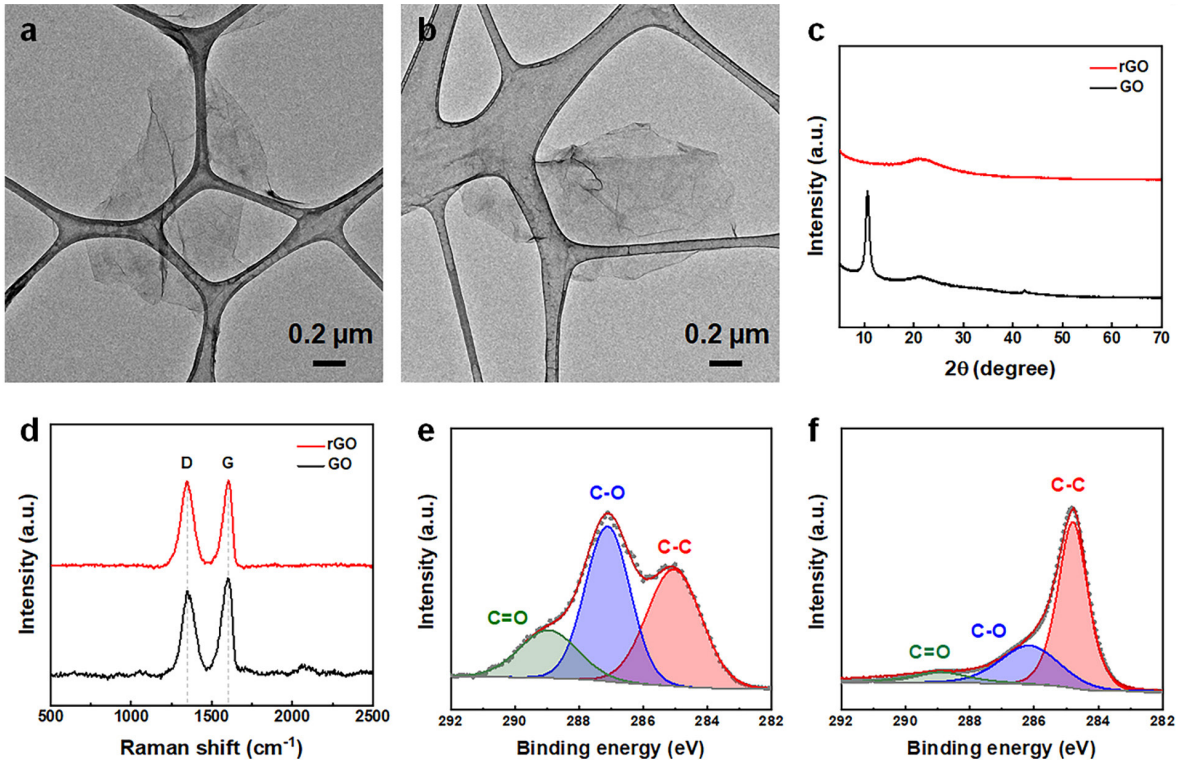

Fig. 2. Transmission electron microscopy image of (a) graphene oxide (GO) and (b) reduced graphene oxide (rGO); (c) X-ray diffraction patterns and (d) Raman spectra of GO and rGO; X-ray photoelectron spectroscopy C 1s spectra of (e) GO and (f) rGO.

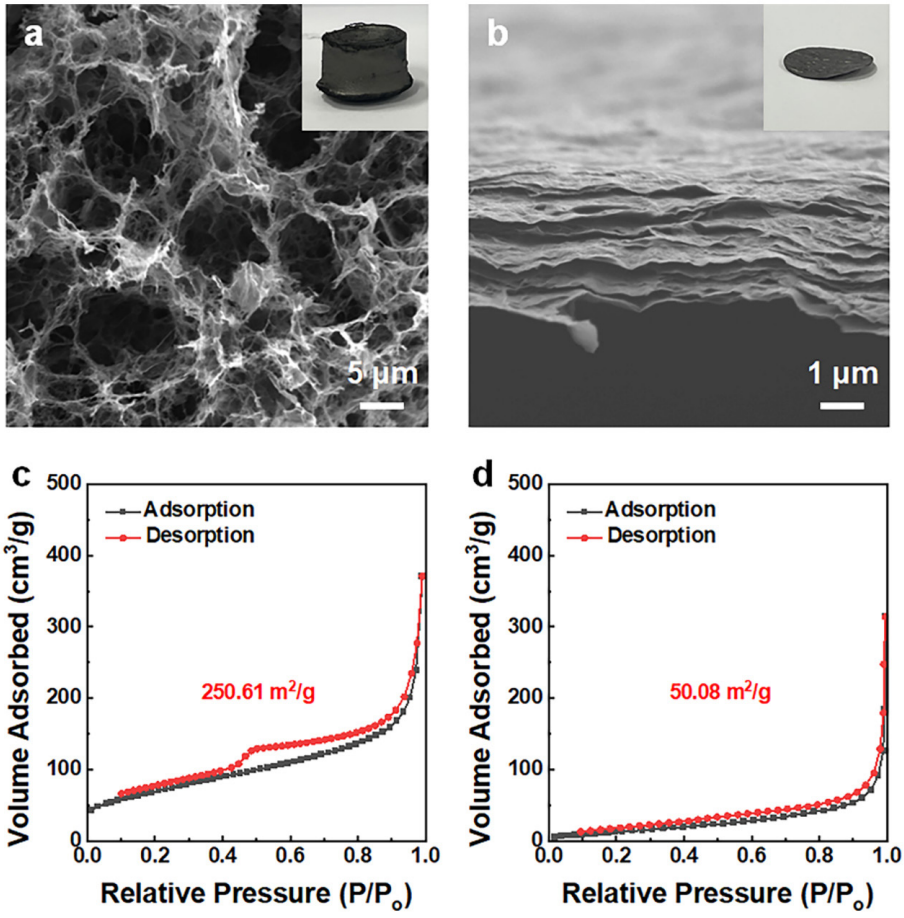

Fig. 3. Scanning electron microscopy images of (a) reduced graphene oxide (rGO) aerogel and (b) rGO film, with digital images shown as insets. N_2 adsorption/desorption isotherms of (c) the rGO aerogel and (d) the rGO film.

the (001) plane [10], indicating the presence of oxygen-containing functional groups and an increased interlayer spacing due to oxidation [11]. After thermal reduction, the (001) peak disappeared and a broad peak appeared at 21.2°, corresponding to the (002) plane, indicating a significant reduction in interlayer spacing, the removal of oxygen groups, and the partial restoration of the sp^2 carbon network [12]. These structural changes, confirmed by XRD analysis, are critical for enhancing the physical and electrochemical properties of rGO. The Raman spectra of GO and rGO (Fig. 2d) provided further insights into the structural changes. Both the GO and the rGO sample exhibited distinct D and G bands. For GO, the I_D/I_G ratio was 0.87, whereas for the thermally reduced rGO the I_D/I_G ratio was higher, 0.99. After thermal reduction, the I_D/I_G ratio increased significantly, indicating partial restoration of the graphene network. Fig. 2e, f shows the XPS spectra of GO and rGO, in which the changes in their chemical composition during the reduction process are apparent. The distinct peaks of the C 1s spectrum of GO corresponded to various carbon-oxygen bonding configurations: the C–C bond at 284.80 eV, the C–O bond at 287.20 eV, and the C=O bond at 289.50 eV [13]. These peaks confirmed the significant presence of oxygen-containing groups, such as hydroxyl, epoxide, and carbonyl. The oxygen atomic percentage of GO was 72.0 at.%, reflecting its high degree of oxidation. After thermal reduction to rGO, the oxygen content decreased significantly, to 36.3 at.%, indicating the partial removal of oxygen functional groups The C 1s spectrum of rGO had a dominant C–C peak at 284.8 eV, suggesting the preservation and partial restoration of the sp^2-hybridized carbon network [13]. For the peaks corresponding to oxygen-containing groups, specifically the C–O and C=O bonds, their intensity was significantly reduced after the reduction process, suggesting partial reduction and restructuring of the oxygen functionalities and thus a transition toward a more graphene-

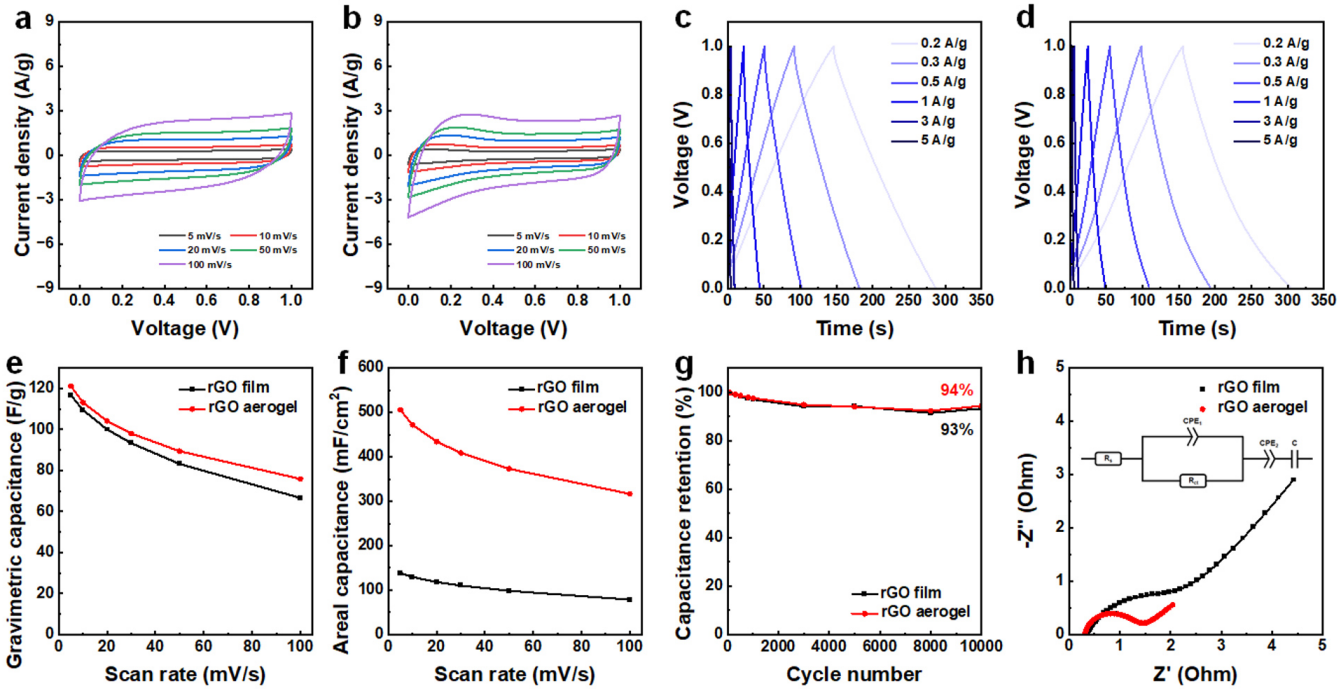

Fig. 4. Electrochemical performance of reduced graphene oxide (rGO) film and aerogel electrodes. Cyclic voltammetry curve at scan rates from 5 mV/s to 100 mV/s for (a) the rGO film and (b) the rGO aerogel. Galvanostatic charge-discharge curves at the current densities from 0.2 A/g to 5 A/g for (c) the rGO film and (d) the rGO aerogel. (e) Gravimetric capacitance and (f) areal capacitance performance comparison. (g) Cycle stability over 10,000 cycles. (h) Nyquist plots showing the electrochemical impedance characteristics.

like structure with fewer oxygen-containing groups.

Fig. 3 shows the microstructures of the rGO aerogel and the rGO film. The highly porous, interconnected network of the rGO aerogel (Fig. 3a) provides abundant ion-accessible sites and facilitates rapid ion transport, which would enhance its electrochemical performance [14]. The rGO film (Fig. 3b), by contrast, has a more compact, layered structure with a distinct lamellar arrangement. The cross-sectional image showed stacked layers, attributable to strong π-π interactions between graphene sheets [15]. This compact layering restricts ion transfer pathways, which can negatively affect capacitance performance [16]. The N_2 adsorption/desorption isotherms of the rGO aerogel and rGO film are shown in Fig. 3c and 3d. The specific surface area of the rGO aerogel was 250.61 m^2/g, significantly larger than the 50.08 m^2/g of the rGO film. This difference reflects the enhanced porosity of the aerogel, which contributes to its superior ion accessibility and electrochemical properties, as compared to the more compact rGO film.

To evaluate the electrochemical performance, symmetric supercapacitor cells were assembled using rGO film and rGO aerogel electrodes. The mass loadings of the rGO film and rGO aerogel electrodes are 1.18 mg/cm^2 and 4.17 mg/cm^2, respectively. CV analysis was performed within a voltage range of 0.0 to 1.0 V. Fig. 4a,b shows the CV curves of the rGO film and aerogel electrodes at scan rates from 5 mV/s to 100 mV/s. Both electrodes yielded nearly rectangular CV shapes even at high scan rates, indicating ideal electric double-layer capacitor behavior. The larger CV curve area of the rGO aerogel electrode reflected the increased availability of ion adsorption sites due to the large specific surface area. The GCD curves are shown in Fig. 4c and 4d. The GCD curves of all electrodes were almost symmetrical and had a triangular shape. The rGO aerogel electrode exhibited a longer discharge time than the rGO film electrode, indicating better capacity performance. The specific capacitance calculated from the CV curve is presented in Fig. 4e and 4f. At a scan rate of 5 mV/s, the rGO aerogel electrode achieved a specific capacitance of 121.2 F/g and 505.6 mF/cm^2, surpassing that of the rGO film electrode (116.7 F/g and 138.2 mF/cm^2). Especially, the rGO aerogel electrode exhibits superior areal capacitance due to its large accessible surface area provided by its porous structure. Cycle stability is presented in Fig. 4g. The capacitance retention of the rGO aerogel electrode was 94% and that of the rGO film

electrode 93%. EIS analysis was employed to investigate the charge transfer dynamics and impedance characteristics over a frequency range of 100 mHz to 100 kHz. The Nyquist plots (Fig. 4h) revealed a smaller semicircle for the rGO aerogel electrode than for the rGO film electrode, indicating a lower charge-transfer resistance, measured as 0.90 Ω for the rGO aerogel electrode and 1.49 Ω for the rGO film electrode. The more efficient charge transfer pathway and lower electron transfer resistance of the rGO aerogel electrode would lead to a superior performance in high-speed charge-discharge processes.

4. Conclusion

This study investigated the synthesis and electrochemical performance of an rGO film and an rGO aerogel as supercapacitor electrodes, revealing the impact of structural design on their properties. The rGO aerogel electrode, with its porous three-dimensional network, exhibited enhanced electrochemical properties, including higher specific capacitance, improved ion transport, and excellent cycle stability. The specific capacitance of the rGO aerogel electrode was 121.2 F/g at 5 mV/s, with 94% of its initial capacitance retained after 10,000 cycles. These properties demonstrated the advantages of the aerogel's open, interconnected structure in facilitating ion accessibility and charge transfer. By contrast, the performance of the rGO film, with its compact, stacked configuration, was limited due to restricted ion diffusion and reduced surface area. These results highlight the critical role of three-dimensional structures in optimizing the performance of supercapacitor materials, by preventing aggregation and enhancing surface accessibility. Based on these findings, rGO aerogels are expected to find broad applicability in energy storage, sensing, and environmental technologies.

Funding

This research was supported by Chungcheongbuk-do Province and Convergence and Open Sharing System (COSS) Development Project (2024).

Conflict of Interest

Dongju Lee serves as an editor of the Journal of Powder Materials editing but has no role in publishing this article. Except for that, the authors declare no competing financial interests or personal relationships.

Data Availability Statement

All dataset files used in this study are already provided in the manuscript.

Author Information and Contribution

Sunghee Choi: MS candidate; conceptualization, writing–original draft. Seulgi Kim: PhD candidate; investigation. Seojin Woo: PhD candidate; visualization. Dongju Lee: Professor; supervision, writing–review & editing, writing–original draft, funding acquisition.

Acknowledgments

None.

References

[1] S. Sharma and P. Chand: Results in Chem., **5** (2023) 100885.
[2] S. Kumar, G. Saeed, L. Zhu, K. N. Hui, N. H. Kim and J. H. Lee: Chem. Eng. J., **403** (2021) 126352.
[3] Y. A. Kumar, G. Koyyada, T. Ramachandran, J. H. Kim, S. Sajid, M. Moniruzzaman, S. Alzahmi and I. M. Obaidat: Nanomaterials, **13** (2023) 1049.
[4] C. Lee, X. Wei, J. W. Kysar and J. Hone: Science, **321** (2008) 385.
[5] S. Stankovich, D. A. Dikin, G. H. Dommett, K. M. Kohlhaas, E. J. Zimney, E. A. Stach, R. D. Piner, S. T. Nguyen and R. S. Ruoff: Nature, **442** (2006) 282.
[6] A. R. Ravindran, C. Feng, S. Huang, Y. Wang, Z. Zhao and J. Yang: Polym., **10** (2018) 477.
[7] R. Heimböckel, F. Hoffmann and M. Fröba: Phys. Chem. Chem. Phys., **21** (2019) 3122.
[8] P. Ramos Ferrer, A. Mace, S. N. Thomas and J.-W. Jeon: Nano Convergence, **4** (2017) 1.
[9] S. Kim, H. Shin, J. Lee, C. Park, Y. Ahn, H.-J. Cho, S. Yuk, J. Kim, D. Lee and I.-D. Kim: ACS Nano, **17** (2023) 19387.
[10] S. Abdolhosseinzadeh, H. Asgharzadeh and H. Seop Kim: Sci. Rep., **5** (2015) 10160.
[11] D. R. Dreyer, S. Park, C. W. Bielawski and R. S. Ruoff: Chem. Soc. Rev., **39** (2010) 228.
[12] C. Gómez-Navarro, J. C. Meyer, R. S. Sundaram, A. Chuvilin, S. Kurasch, M. Burghard, K. Kern and U. Kaiser: Nano Lett., **10** (2010) 1144.
[13] H. Xu, Z. Liu, C. Qiao, X. Zhang, Q. Zhang, Y. Zhang and Y.

Zheng: J. Appl. Polym. Sci., **140** (2023) e53502.
[14] C. Tang, H.-F. Wang, J.-Q. Huang, W. Qian, F. Wei, S.-Z. Qiao and Q. Zhang: Electrochem. Energy Rev., **2** (2019) 332.
[15] P. Piotrowski, A. Fedorczyk, J. Grebowski and A. Krogul-Sobczak: C J. Carbon Res., **8** (2022) 17.
[16] A. Subramanian, B. George, S. R. Bobbara, I. Valitova, I. Ruggeri, F. Borghi, A. Podestà, P. Milani, F. Soavi and C. Santato: AIP Adv., **10** (2020) 065314.